

## Performance of TRISO particles fueled with plutonium and minor actinides in a PBMR-400 core design

J. Jonnet\*, J.L. Kloosterman, B. Boer<sup>1</sup>

Delft University of Technology, Reactor Institute Delft, Mekelweg 15, 2629 JB Delft, The Netherlands

### ARTICLE INFO

#### Article history:

Received 4 November 2009

Received in revised form 29 January 2010

Accepted 1 March 2010

### ABSTRACT

The TRISO particle design of high temperature reactors fueled with plutonium (Pu) and/or minor actinides (MAs) is investigated by calculating the failure fraction of TRISO particles during irradiation. For this purpose, a fuel depletion, neutronics and thermal-hydraulics code system, which delivers the fuel temperature, fast neutron flux and power density profiles, is coupled to an analytical stress analysis code. The latter is being further developed for the calculation of a reliable and realistic failure fraction. The code system has been applied to a PBMR-400 design containing TRISO particles fueled with 1st and 2nd generation plutonium and with a target burn-up of 700 and 600 MWd/kgHM, respectively. It is shown that the pebble-bed type high temperature reactor under consideration is a promising option for burning Pu and MAs if very high burn-ups can be achieved. The TRISO particle failure fraction is also calculated for both Pu and MA fuels, and compared to U-based fuel. It is shown by the present stress analysis code that the Pu-based fuel particles need a better design and this has been achieved for the MA-based fuel, in which helium gas atoms have a significant contribution to the buffer pressure.

© 2010 Elsevier B.V. All rights reserved.

### 1. Introduction

The sustainability of the nuclear fuel cycle and the reduction of plutonium (Pu) and minor actinides (MA) stockpiles are key issues in the definition of the future nuclear energy mix in Europe. The high temperature gas-cooled reactor (HTR) can incinerate both Pu and MA due to its unique and unsurpassed safety features.

Apart from the inherent safety features offered by this reactor type, the nature of the coated particle fuel offers a number of attractive features. In particular, it can withstand burn-ups far beyond that in either LWR or fast reactor systems, as demonstrated in former tests (Alberstein, 1994).

The PUMA project is a Specific Targeted Research Project of the European Union EURATOM 6th Framework Program and, complementary with other initiatives, mainly aims at providing additional key elements for the utilisation and transmutation of plutonium and minor actinides in high temperature gas-cooled reactor designs (Kuijper, 2007).

Within PUMA, new coated particle designs for Pu/MA incineration will be explored. For this purpose, helium and swelling behavior models for coated Pu and MA particle fuels together

with fuel performance models, appropriate to HTR fuels, need to be further developed. Finally, the impact of such an utilisation of the HTR on economics and the entire fuel cycle will be assessed.

Delft University of Technology (TU-Delft) participated in the optimisation of the fuel design of HTRs fueled with plutonium and/or minor actinides. To this end, the failure fraction of TRISO coated fuel particles is calculated during irradiation by coupling a neutronics, fuel depletion and thermal-hydraulics code system (Boer et al., 2010), which will deliver the fuel temperature, burn-up and power density profiles, to an in-house developed stress analysis code called CRYSTAL (Code foR analysis of STresses in coAted particles) (Boer et al., 2008). The calculation scheme is depicted in Fig. 1. Unlike in other codes (PANAMA Nabielek et al., 2004 and PARFUME Miller et al., 2008 for instance), direct coupling of core physics code to fuel performance enables the analysis and design of TRISO particles from non-constant irradiation conditions, and as realistic as possible depending on the core geometry used and accuracy of core physics codes. In the following, all calculations are limited to the case of the pebble-bed reactor core, although calculations for other core geometries are also possible.

In Section 2, the stress analysis code CRYSTAL is presented. The main governing equations of the code that was first reported in literature (Boer et al., 2008) are briefly presented. New developments of the code are then proposed in Section 3. Section 4 of the present paper refers to the application of the fuel performance code system (core physics code coupled to the stress analysis code) to a PBMR-

\* Corresponding author. Current address: Nuclear Research and consultancy Group, Safety & Power, PO Box 9034, 6800ES Arnhem, The Netherlands. Tel.: +31 263568515; fax: +31 263518536.

E-mail address: [jonnet@nrg.eu](mailto:jonnet@nrg.eu) (J. Jonnet).

<sup>1</sup> Current address: Idaho National Laboratory, Idaho Falls, USA.

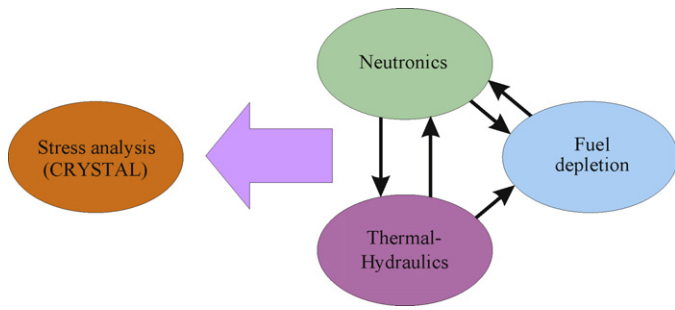


Fig. 1. Fuel performance model overview.

400 core design, fueled with 1st and 2nd generation plutonium. In the second case, the fuel is diluted in an yttria-stabilised zirconian inert matrix. The equilibrium composition states are calculated and shown, as well as the capability of the pebble-bed reactor to burn plutonium and minor actinides. Section 5 of the paper is dedicated to the fuel performance calculations of the two fuel compositions under consideration. Several cases are considered, in order to show the influence of important mechanisms such as fission gas release or cracking of the Pyrocarbon layers. Stresses in the coating layers are shown and failure fractions are calculated. In Section 6 of this paper, the results are summarised and the perspectives of the fuel performance code are discussed.

## 2. Development of a stress analysis code for TRISO particles

The Code foR anaLYsis of STresses in coAted particLes (CRYSTAL) has been developed to calculate the stresses in the different layers of the coated particles and surrounding graphite (referred as a 4th layer) during irradiation. This code is an extension of existing analytical models (Miller and Bennett, 1993) based on viscoelastic description of stresses, and is able to quantify many stress phenomena (Boer et al., 2008). Although it was shown that the graphite matrix surrounding the coated particles has some effects on the stress in the coatings (Boer et al., 2007, 2008), the 4th layer is not taken into account in the present analysis. This is mainly due to the combination with another structural failure mechanism, through the introduction of a crack-induced failure model (see Section 3.3), which complicates the mathematical development and analysis.

### 2.1. Governing equations of stresses in TRISO particle coating layers

The creep behavior in the pyrocarbon layers of the fuel particle and the graphite matrix can be modelled with a Maxwell creep model. The latter assumes that the steady state strain rate can be represented by an elastic (spring) and viscous (dashpot) model in series (Miller, 1995). The strain derivatives for the radial and tangential directions in a spherical element, including irradiation-induced creep and dimensional change, and thermal expansion, read:

$$\frac{\partial \varepsilon_r}{\partial t} = \frac{1}{E} \left[ \frac{\partial \sigma_r}{\partial t} - 2\mu \frac{\partial \sigma_t}{\partial t} \right] + c [\sigma_r - 2\nu\sigma_t] + \alpha_r \dot{T} + \dot{S}_r \quad (1)$$

$$\frac{\partial \varepsilon_t}{\partial t} = \frac{1}{E} \left[ (1 - \mu) \frac{\partial \sigma_t}{\partial t} - \mu \frac{\partial \sigma_r}{\partial t} \right] + c [(1 - \nu)\sigma_t - \nu\sigma_r] + \alpha_t \dot{T} + \dot{S}_t \quad (2)$$

From the strain-displacement relations and equilibrium requirement follows (Timoshenko and Goodier, 1970):

$$\varepsilon_r = \frac{\partial u}{\partial r} \quad (3)$$

$$\varepsilon_t = \frac{u}{r} \quad (4)$$

$$\frac{\partial \sigma_r}{\partial r} = \frac{2}{r} (\sigma_t - \sigma_r) \quad (5)$$

where  $u$  is the radial displacement.

### 2.2. Solutions of radial displacements and stresses in TRISO particle coating layers

In order to find the solutions of Eqs. (1)–(5), the same procedure is used as in Miller (2006). The closed form solution in Miller (2006) is an improvement over the earlier solution found in Miller (1995) and allows the material properties to change with irradiation time (or dose). Furthermore, the solution allows for the Poisson's ratio of creep to deviate from  $\nu = 0.5$ . The solutions for the radial displacement and for the radial and tangential stresses are assumed to be in form of series (Miller and Bennett, 1993):

$$u(r, t) = \sum_{i,n=0}^{\infty} u_{i,n} t^n \quad (6)$$

$$\sigma_r(r, t) = \sum_{i,n=0}^{\infty} \sigma_{r,i,n} t^n \quad (7)$$

$$\sigma_t(r, t) = \sum_{i,n=0}^{\infty} \sigma_{t,i,n} t^n \quad (8)$$

Once Eqs. (1)–(8) have been combined together, the following method is applied:

- Calculation of the radial displacements at the layer interfaces: the boundary conditions at each layer interface imply continuity of radial stress and displacement. The incremental solution for the displacement  $u_i$  can be found (Miller and Bennett, 1993) (not detailed here for sake of brevity). By inserting the latter solution into the incremental form of the equilibrium Eq. (5), a general expression for the displacement in a spherical layer is found.
- Calculation of radial stresses at the layer interfaces. By use of the continuity of radial displacements at all layer interfaces and after differentiation with respect to  $t$ , a system of three inhomogeneous linear equations for the radial stress at the interfaces is obtained.
- Calculation of the radial and tangential stresses at any position within the layers.

### 2.3. Irradiation effects in the coating layers during irradiation

Fission products are formed during irradiation within the fuel kernel. Among them, the gaseous fission products diffuse to and accumulate in the buffer layer, contributing directly to the pressure build-up which depends on the kernel temperature and buffer volume. Another contribution to the pressure is provided by the formation of CO gas in the buffer. The buffer pressure is the main source of stress in the coating layers.

Moreover, and as introduced in Eqs. (2) and (1), the layers undergo irradiation-induced creep and dimensional change.

The equations for these effects are presented below.

#### 2.3.1. Pressure build-up in the buffer layer

The release-to-birth ratio of stable (long-lived) fission gases from the kernel is calculated by a numerical method, which solves

the diffusion equation from an equivalent sphere of radius  $a$ :

$$\frac{\partial C}{\partial t} = \frac{D}{r^2} \left[ \frac{\partial}{\partial r} \left( r^2 \frac{\partial C}{\partial r} \right) \right] + \beta \quad (9)$$

where  $C$  is the fission gas concentration (atoms  $\text{m}^{-3}$ ),  $D$  the atom diffusion coefficient ( $\text{m}^2 \text{s}^{-1}$ ),  $\beta$  the stable fission gas production rate (atoms  $\text{m}^{-3} \text{s}^{-1}$ ). The numerical approach is, most of the time, preferred to solve Eq. (9). It allows for a non-zero concentration at the boundary, which is an improvement compared to the analytical approach in which a zero concentration in the porous buffer layer is usually assumed throughout the irradiation period (Olander, 1976).

The source term is initially determined by the local power (burn-up rate) in the reactor. From the fuel depletion analysis with ORIGEN (ORNL, 2005) it is found that approximately one third of the fission products in  $\text{UO}_2$  particle fuel are gaseous stable xenon and krypton atoms, which compares well with the value (31%) used by Nabilek et al. (2004).

Besides direct formation of gaseous fission products, formation of CO gas by a reaction of oxygen present in the fuel kernel and carbon in the buffer layer is possible. The formation of this gas in U-based TRISO particles is taken into account by the following empirical formula (Proksch et al., 1982; Nabilek et al., 2004) for oxygen release per fission:

$$\frac{O}{f} = 8.32 \times 10^{-11} t_{\text{irr}}^2 e^{\left(\frac{-Z}{RKT}\right)} \quad (10)$$

In Eq. (10),  $O/f$  is the number of oxygen atoms released per fission, after an irradiation time  $t_{\text{irr}}$  (s);  $Z$  has the value  $162.7 \text{ kJ mol}^{-1}$ ,  $R$  is the universal gas constant ( $8.314 \text{ J mol}^{-1} \text{ K}^{-1}$ ) and  $T$  is the temperature (K). It is emphasised that no reliable data for the CO gas formation in Pu and PuMA-based TRISO fuels is available, Eq. (10) is only applicable to U-based TRISO fuels. However, this problem has been alleviated in the present analysis by proposing in Section 4 hypo-stoichiometric fuel kernels. As a result, the CO gas formation and contribution in the buffer pressure can be considered as negligible as a first approximation (see Section 5).

The resulting pressure in the buffer layer that acts on the iPyC layer is calculated with the Redlich–Kwong equation of state (Smith et al., 2001), as a function of the kernel temperature, buffer volume and total gas inventory in the buffer:

$$RT_{\text{kernel}} = \left( P + \frac{a}{T_{\text{kernel}}^{\frac{1}{2}} V_m (V_m + b)} \right) (V_m - b) \quad (11)$$

The ideal gas law is not applied, because it under-predicts the pressure significantly (I-NERI, 2004).

### 2.3.2. Dimensional change and creep of particle coatings

Under irradiation, the PyC layers are exposed to a fast neutron flux, which causes dimensional changes. The dimensional change rate depends on the initial density and anisotropy of the pyrocarbon material. Several empirical relations for the radial and tangential dimensional change rate exist (I-NERI, 2004). In general the layers shrink at low neutron dose. This shrinking eventually stops at higher irradiation dose. In some cases, depending on the material properties, the shrinking turns into swelling at higher doses. The following relations are adopted in the present fuel performance model (I-NERI, 2004):

$$\dot{S}_r = -0.077e^{(-t)} + 0.031 \quad (12)$$

$$\dot{S}_t = -0.036e^{(-2.1t)} - 0.01 \quad (13)$$

In these relations  $\dot{S}_r$  and  $\dot{S}_t$  are the dimensional change rates in the radial and tangential directions, respectively, expressed in

$(10^{25} \text{ m}^{-2})^{-1}$  and  $t$  is the fast neutron fluence (for energies  $E > 0.1 \text{ MeV}$ ) expressed in  $10^{25} \text{ m}^{-2}$ .

Moreover, pyrocarbon and graphite materials creep under irradiation, partly reducing the stress. For the pyrocarbon layers a value of  $2.0 \times 10^{-29} (\text{MPa m}^{-2})^{-1}$  is taken for the creep coefficient from literature (I-NERI, 2004). Oku et al. (1990) and Oku and Ishihara (2004) determined the irradiation creep coefficient for HTGR (matrix) graphite to be in the range of  $3.4 \times 10^{-29}$ – $4.8 \times 10^{-29} (\text{MPa m}^{-2})^{-1}$  (for  $E > 0.18 \text{ MeV}$ ) at 1029–1257 K, with an average value of  $4.2 \times 10^{-29} (\text{MPa m}^{-2})^{-1}$ .

## 3. Further development of the stress analysis code CRYSTAL

### 3.1. Thermal expansion of TRISO coating layers

Although taken into account in the governing equations of the analytical 4-layer model (Eqs. (1), (2) and (5)), thermal expansion of the PyC and SiC layers was initially set to zero.

For the case of the pyrocarbon layers, it is here proposed to follow the work of Wang (2004) to provide the model with thermal expansion coefficients that depend on the layer anisotropy. For a non-porous aggregate of hexagonal crystallites, the thermal expansion coefficient in a direction X is given by the expression taken from Bacon (1956):

$$\alpha_x = R_x \alpha_a + (1 - R_x) \alpha_c \quad (14)$$

where  $\alpha_a$  and  $\alpha_c$  are the crystallite expansion coefficients in the  $a$  and  $c$  directions and  $R_x$  is a preferred orientation parameter. For the OZ direction (the axis of symmetry, perpendicular to the deposition plane) and the OX direction (parallel to the deposition plane),  $R_z$  and  $R_x$  are defined by:

$$R_x = 1 - \frac{R_z}{2} \quad (15)$$

and  $R_z$  is the parameter that characterizes the preferred orientation, referred to the normal to the deposition plane OZ. Note that in the case of a spherical particle, the normal to the deposition plane OZ corresponds to the radial direction, and OX to the tangential direction. The Bacon Anisotropy Factor (BAF) is also related to  $R_z$ :

$$BAF = 2 \left( \frac{1 - R_z}{R_z} \right) \quad (16)$$

However, it is found that the actual thermal expansion of pyrocarbon deviates from the Bacon relation, given by Eq. (14). Wang (2004) finally proposed the following thermal expansion coefficient for pyrocarbons layers, also reported in I-NERI (2004), to be:

$$\alpha_r = -\frac{125}{3} R_z + \frac{100}{3} \quad (17)$$

$$\alpha_t = 40(R_x - 1)^2 + \frac{10}{9} \quad (18)$$

where  $R_z$  and  $R_x$  are given by Eqs. (16) and (15), respectively.  $\alpha_r$  and  $\alpha_t$  are in  $\text{K}^{-1} (\times 10^{-6})$ .

The thermal expansion coefficient of the silicon carbide layer is found to show no systematic dependence on the deposition temperature and is not affected by neutron irradiation (I-NERI, 2004).

For the present analysis, a Bacon Anisotropy Factor (BAF) equal to 1 is applied. Although it is well accepted that no Pyrocarbon on coated particles is completely isotropic, the BAF depends on the fabrication process. Moreover, the CRYSTAL code does not contain so far any other anisotropy-dependent properties, which may also change during irradiation. As a consequence, a BAF equal to 1 is only used here as a starting point in the present analysis. This results in the following radial and tangential thermal expansion coefficients for both inner and outer Pyrocarbon layers:

$$\alpha_r = \alpha_t = 5.55 \times 10^{-6} \text{ K}^{-1} \quad (19)$$

For the SiC layer, a thermal expansion coefficient equal to  $4.9 \times 10^{-6} \text{ K}^{-1}$  is used (CEGA, 1993). Effect of neutron irradiation on anisotropy is not taken into account in the CRYSTAL code due to the lack of reliable data. However, since the iPyC and oPyC layers expand more than the SiC layer, the tangential stress in the SiC layer is expected to increase with increasing anisotropy.

### 3.2. Stable fission gases and helium release models in Pu/MA-based fuel particles

Although the numerical method allows non-zero boundary conditions and is very accurate, the computation time can be an issue (see next section). An alternative solution is based on an analytical method provided by Kidson (1980), which is especially adapted to non-constant conditions (multiple cycles):

$$F^k(t) = 1 - \sum_{n=1}^{\infty} \left[ \frac{6a^2}{n^4 \pi^4} \times \sum_{s=1}^k \frac{\beta^s}{D^s} (1 - \exp(-\phi^s)) \times \exp(-\Delta\Phi^{ks}) \right] \times \left[ \sum_{s=1}^k (\beta t)^s \right]^{-1} \quad (20)$$

where  $F^k(t)$  is the release-to-birth ratio of fission gases at cycle  $k$ ,  $\phi = n^2 \pi^2 (Dt/a^2)$  and  $\Delta\Phi^{ks} = \sum_{r=s}^k \phi^r$ . In the latter equations, the superscripts  $k$ ,  $s$  and  $r$  are not an exponent but refer to the cycle number. The last summation in Eq. (20) is simply the total gas atom production during all  $k$  cycles. In practice,  $n$  is chosen to provide both fast calculations and good accuracy.

A very cheap option in computation time consists of an approximate solution that was deduced from the well-known Booth solution in constant irradiation conditions and extended in the CRYSTAL code to cyclic irradiation history for the cumulative release  $f$ :

$$f = 4 \left( \frac{Dt}{\pi a^2} \right)^{1/2} - \frac{3}{2} \left( \frac{Dt}{a^2} \right) \quad (21)$$

In Eq. (21), the  $(Dt)$  terms contain the temperature dependence of the irradiation history and are simply accumulated from one cycle to another. Eqs. (20) and (21) are used in a sensitivity analysis in order to determine the effect of the buffer pressure on the final failure fraction.

The calculation of the buffer pressure also includes the contribution of helium. As a first step, it is assumed that 100% helium is released at the considered kernel temperature. This assumption is conservative although the production of helium in the 1st generation plutonium fuel is still one order of magnitude less than stable xenon and krypton, as calculated with the present code system. On the other hand, helium may have a higher contribution to the buffer pressure build-up in the case of the 2nd generation plutonium fuel. The helium behavior will need to be improved by integrating an empirical model for helium swelling and release in Pu/MA HTR fuels.

### 3.3. Effects of PyC cracking on TRISO particle mechanical behavior

The SiC layer provides retention of all fission products under normal operating conditions. It acts as a pressure vessel and is modelled as such in many codes (see for instance in Sawa et al. (1996)). When the stress in the SiC layer is tensile and high enough, the layer is said to fail due to over-pressure. Recently, Wang and Ballinger (2004) proposed a model in which PyC layers can fail first (due to over-pressure), creating a radial crack. This results in an increase in the local stress at the PyC/SiC interface and produces a local crack tip stress intensity  $K_I^{SiC}$ . Although the effect of PyC cracking is not well quantified, cracked PyC layers were observed

in some past irradiation experiments, for instance in the Deep Burn irradiation experiments at Peach-Bottom-1 MHR. From these past experiments, it seems that PyC cracking may be related to highly excessively anisotropic pyrocarbons. Although today's fuel specifications will tend to prevent such a behavior during irradiation, this has to be also proven theoretically via the development of specific models in fuel performance codes.

If the value of  $K_I^{SiC}$  exceeds the fracture toughness ( $K_{IC}$ ) of the SiC layer then the layer fails even when the far field stress in the SiC is compressive. The model was called the "crack-induced failure model" by its authors. For instance, the calculation of the mode I stress intensity factor in the SiC layer due to a cracked iPyC layer reads:

$$K_I^{SiC} = K_I^{iPyC}(t) \sqrt{\frac{d}{a_{iPyC}}} + \bar{\sigma}_{SiC}(t) \sqrt{\pi d} \quad (22)$$

In Eq. (22),  $d$  is the SiC grain diameter,  $a_{iPyC}$  is the crack length in the iPyC layer,  $\bar{\sigma}_{SiC}(t)$  is average circumferential stress in the SiC layer, and  $K_I^{iPyC}(t)$  is the Mode I stress intensity factor in the radially cracked iPyC layer.

The crack-induced failure model proposed by Wang and Ballinger (2004) has been implemented in the CRYSTAL code and is used to assess the effect of a PyC layer failure on the TRISO particle failure fraction during irradiation. By considering that both iPyC and oPyC layers can fail, many failure scenarios must be taken into account, as shown in Fig. 2.

### 3.4. Monte Carlo sampling of particle geometry and material properties

By use of the analytical stress analysis code (Boer et al., 2008), the stress field in all coating layers can be calculated as a function of fast neutron fluence. This allows the failure probability to be calculated, for instance with the widely used Weibull distribution function (Sawa et al., 1996):

$$P = 1 - \exp \left( - \ln 2 \left( \frac{\sigma_t}{\sigma_{med}} \right)^m \right) \quad (23)$$

$\sigma_t$  and  $\sigma_{med}$  are the maximum tangential (tensile) stress and median strength in the SiC layer, respectively.  $m$  is the Weibull modulus.

However, Eq. (23) gives the failure probability of the mean or nominal TRISO particle, which is different from the average failure fraction of all particles that are being irradiated in the core. The two methods for the calculation of failure probability/fraction differ because of the statistical variations of the TRISO geometry and material properties that occur during the fabrication process. In order to take this into account, Monte Carlo (MC) sampling has been deployed.

In such techniques, the size of the sample plays a major role. In order to calculate a failure fraction as low as  $10^{-6}$  with good accuracy, the modeler should make use of a sample of  $10^8$  particles with Direct Monte Carlo method. Advanced MC techniques aim at increasing the accuracy for the same sample size, or equivalently at decreasing the sample size for a given accuracy (here  $10^{-6}$ ). For instance, the sample size can be reduced to  $10^6$  particles in Conditional Monte Carlo, and to  $10^5$  particles in Importance Sampling MC (Michel, 2007). However, as highlighted in Section 3.3 and shown in Fig. 2, the crack-induced failure model introduces many possibilities for the SiC layer to fail. As a consequence, only the Direct MC method is suitable here to calculate the failure fraction of TRISO particles.

Once the sampling method is selected, the next step consists in choosing the most realistic distributions for the particle geometry and mechanical property. For this purpose, the truncated Gaussian distribution is chosen for sampling the kernel diameter and

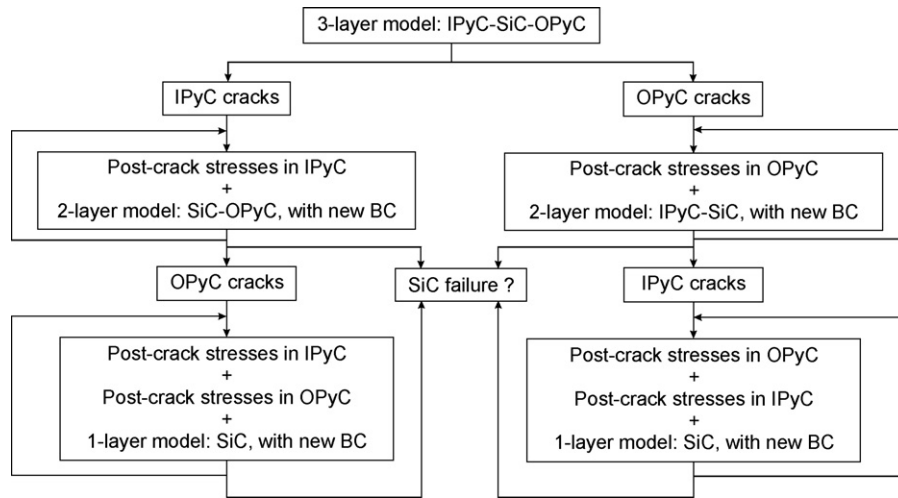


Fig. 2. Flow diagram showing the possible scenarios of the crack-induced failure model.

all coating layer thicknesses, which are calculated as follows:

$$x = \mu + \sigma\sqrt{2} \operatorname{erf}^{-1} \left[ \operatorname{erf} \left( \frac{a - \mu}{\sigma\sqrt{2}} \right) + \left( \operatorname{erf} \left( \frac{b - \mu}{\sigma\sqrt{2}} \right) - \operatorname{erf} \left( \frac{a - \mu}{\sigma\sqrt{2}} \right) \right) \times R \right] \quad (24)$$

where  $x$  is the value of the parameter that follows the truncated Gaussian distribution,  $a$  and  $b$  are the lower and upper bound of the possible values for  $x$ , respectively.  $\mu$  and  $\sigma$  are the mean value and standard deviation, respectively,  $\operatorname{erf}$  is the error function, and  $R$  is a random number.

The two-parameter Weibull distribution is preferably used to sample the value of the characteristic strength of the coating layers, which is given by:

$$x = \mu \exp \left( \frac{\ln(-\ln R)}{\sigma} \right) \quad (25)$$

The variables in Eq. (25) have the same meaning as in Eq. (24).

Table 1 shows the values used in the truncated Gaussian and Weibull distributions when the MC technique is applied.

#### 4. Application to a PBMR-400 core design

In the following, all calculations are limited to the case of the pebble-bed reactor core, although calculations for other core geometries are also possible. In particular, all calculations are performed for the case of the PBMR-400 reactor. The next step consists in choosing the fuel composition that will be loaded in the core.

Table 1  
Distribution parameters.

Property	Mean value	Standard deviation
Kernel diameter ( $\mu\text{m}$ )	200 <sup>a</sup> /500 <sup>b</sup>	11 <sup>c</sup>
Buffer thickness ( $\mu\text{m}$ )	90 <sup>a</sup>	14 <sup>c</sup>
iPyC thickness ( $\mu\text{m}$ )	40 <sup>a</sup>	4 <sup>c</sup>
SiC thickness ( $\mu\text{m}$ )	35 <sup>a</sup>	2.5 <sup>c</sup>
oPyC thickness ( $\mu\text{m}$ )	40 <sup>a</sup>	3 <sup>c</sup>
iPyC charact. strength ( $\text{MPa m}^{3/\beta}$ )	24 <sup>d</sup>	9.5 <sup>d</sup>
SiC charact. strength ( $\text{MPa m}^{3/\beta}$ )	9.64 <sup>d</sup>	6.0 <sup>d</sup>
oPyC charact. strength ( $\text{MPa m}^{3/\beta}$ )	24 <sup>d</sup>	9.5 <sup>d</sup>

<sup>a</sup> Taken from Alberstein (1994)

<sup>b</sup> Usual values for U-fuel TRISO particles (Boer et al., 2008)

<sup>c</sup> Taken from Heit et al. (1984)

<sup>d</sup> Taken from Wang et al. (2004)

#### 4.1. Choice of the PuMA reference fuels

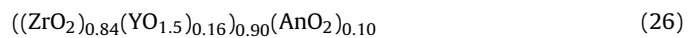
Based on past Pu-burning experiments at Peach-Bottom (Alberstein, 1994), in which  $\text{PuO}_{1.7}$  fuel kernels of 200  $\mu\text{m}$  diameter were irradiated up to very high burn-ups, the starting fuel for all analyses in the PUMA project was chosen to be  $\text{PuO}_{1.7}$  fuel kernels containing first generation plutonium (i.e. from recycled LWR  $\text{UO}_2$  fuel). The isotopic composition vector is given in Table 3. In the following, this fuel is referred as the 1st reference fuel.

In the case of a pebble-bed type HTR, preliminary results were obtained with the use of (U-free) Pu-containing coated particle fuel in a contemporary design of the PBMR-400 pebbled-bed HTR operating in continuous multi-pass refuelling mode (de Haas et al., 2006), where it was assumed that each fresh fuel pebble contains 2 g first generation Pu in coated particles with a kernel diameter of 240  $\mu\text{m}$ .

Calculations performed so far by use of the PANTHERMIX code on a Pu-loaded HTR-MODULE (Kuijper et al., 2004) show that a discharge burn-up of about 740 MWd/kgHM can be reached with 67% fissile Pu (1st generation, see Table 3), where  $k_{\text{eff}}$  is still slightly above 1 in the equilibrium (fuel mixture) state. In the present paper, the calculation of equilibrium state has been performed with a target burn-up of 700 MWd/kgHM, which should correspond to a value achievable without any particular optimisation of the core.

However and as highlighted by Kuijper (2007), the reference plutonium oxide kernel with a diameter of 200  $\mu\text{m}$  may not be the best choice, and is based largely on historical reasons. A much better option could consist of actinide infiltration into a porous precursor kernel. This minimizes wastes and reduces the handling steps involving minor actinides. In these conditions and although not being the utmost priority of the PUMA project, MA-based fuel should also be studied, in order to propose as many fuel cycle scenarios as possible. As a result, a second reference fuel containing minor actinides diluted in an inert matrix has been selected.

Although many options are possible depending on the fuel and inert matrix combinations (Somers, 2007), the following fuel composition is proposed:



with An taken from recycled PWR spent fuel after five years of cooling, as shown in Table 2.

The yttria-stabilised zirconia matrix in Eq. (26) has been selected due to its past experience as an inert matrix (especially with  $\text{Y}/(\text{Y} + \text{Zr}) = 16$  mol%). More details on the fuel preparation and characterization can be found in Somers and Fernandez (2006) and

**Table 2**  
Alternative reference fuel composition (Mignanelli, 2008).

Nuclide	Fraction (wt.%)
Np-237	6.8
Pu-238	2.9
Pu-239	49.38
Pu-240	23.0
Pu-241	8.8
Pu-242	4.9
Am-241	2.8
Am-242m	0.02
Am243	1.4

Walter et al. (2007). As far as proliferation resistance is concerned (Hesketh, 2007), this is a very good option as this inert matrix is difficult to reprocess. Moreover, it provides a good option for fuels to be sent directly for geological disposal (Grambow et al., 2007).

The molar fraction of the minor actinide oxide  $AnO_2$  was initially calculated to be 5 mol%. This corresponded to a mass content of 9.9 wt.% of minor actinides in the fuel kernel. The latter value was derived from the past Pu-burning experiments at Peach-Bottom. In this experiment, the  $PuO_{1.7}$  kernel of 200  $\mu m$  in size contained 0.041 mg of Pu. By using the yttria-stabilised zirconia matrix, a 500  $\mu m$  diameter kernel with the same Pu mass would give a Pu fraction (over the total oxide mass) of 9.9 wt.%. The same calculation is applicable to MA fuel (Somers and Fernandez, 2007). However, such a low fraction of minor actinides in the fuel kernel would entail both a low power per TRISO particle and a high packing fraction of TRISO particles per pebble (to keep constant the heavy metal mass per pebble). As a result, the fraction of  $AnO_2$  was increased to 10 mol%, and the packing fraction therefore decreased from 29.4% to 14.7%. The number of TRISO particles per pebble with this fuel composition is calculated to be 26750, to be compared to 48820 particles for the  $PuO_{1.7}$  fuel. For sake of clarity with other Work Package analyses within the PUMA project, the present fuel is referred as the *advanced reference fuel*, and the molecular composition given in Eq. (26) is mentioned as  $(Y,Zr,An)O_2$ .

For the advanced reference fuel, the target discharge burn-up has been calculated to be around 600 MWd/kgHM.

#### 4.2. Equilibrium state of the Pu/MA-loaded PBMR-400 core

A core physics calculation procedure has been developed (Boer et al., 2010) and makes use of existing and well documented codes or modules, such as SCALE-5 (ORNL, 2005) and THERMIX (Struth, 1995), and of a neutron diffusion code DALTON that proved to provide good results in benchmark exercises (Boer et al., 2010).

Modules of SCALE-5 are used for the fuel depletion calculation and cross-section generation. THERMIX is a 2D thermal-hydraulics code that enables, when coupled to the cross-section generation script and diffusion code DALTON, to obtain a temperature-dependent cross section library and consequently a temperature-corrected power profile.

Figs. 3(a) and (b) and 4(a)–(c) show the solid temperature of the reactor, the gas temperature, fast and thermal neutron fluxes and power density in the core, respectively, when the PBMR-400 core loaded with the 1st reference fuel is in the equilibrium composition state at a target burn-up of 700 MWd/kgHM.

It is shown that all calculated distributions are comparable to the ones reported in de Haas et al. (2006) and Kuijper et al. (2004). The high temperature at the bottom of the inner reflector, high outlet gas temperature and power density peaks below the top of the core and located close to the inner and outer reflectors are particularly noticed. Moreover, the latter results are shown to be similar to the ones obtained when the PBMR-400 core is loaded with  $UO_2$

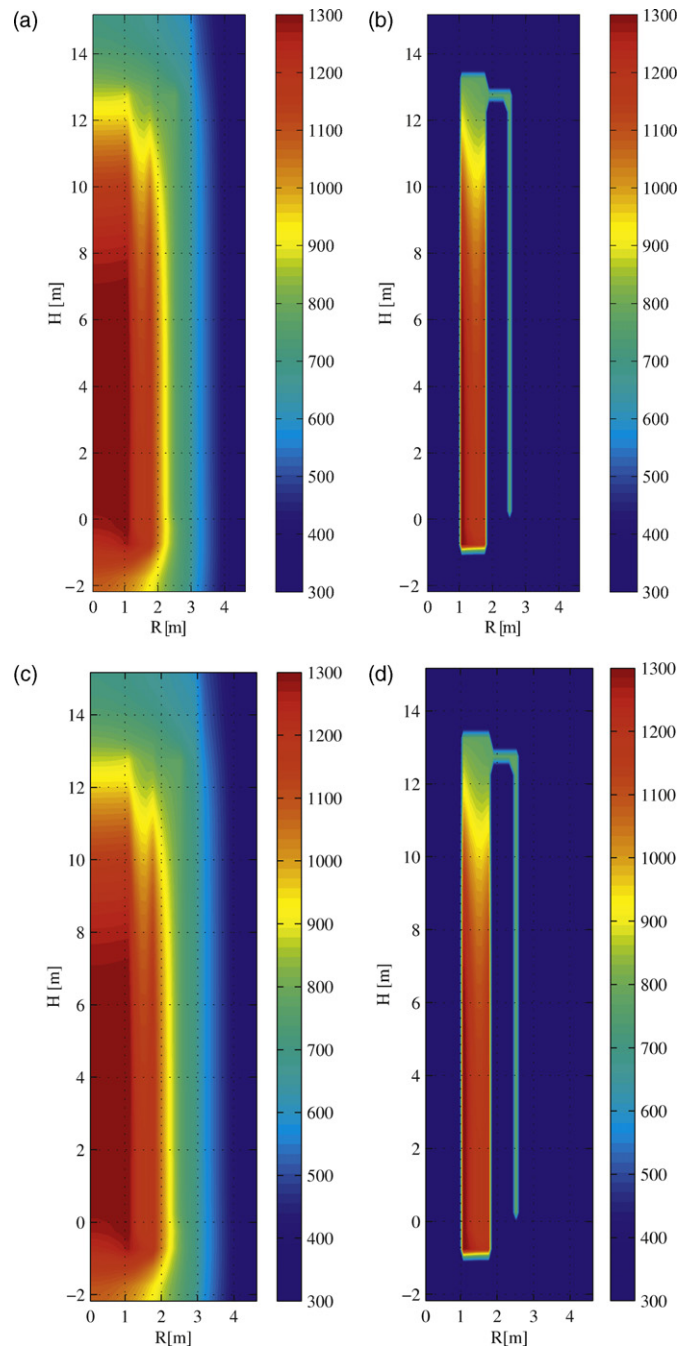


**Fig. 3.** (a and c) Solid and (b and d) gas temperatures (K) in the reactor for the 1st and advanced reference fuels, respectively.

fuel elements. A direct comparison can be found in Refs. Boer et al. (2008) and Jonnet et al. (2008).

The same calculation procedure for the equilibrium composition state was applied to the advanced reference fuel, at a target discharge burn-up of 600 MWd/kgHM. The results are shown in Figs. 3(c) and (d) and 4(d)–(f). It is shown that the solid and gas temperatures of the reactor are very similar for the 1st and advanced reference fuels. However, in the case of the advanced reference fuel the peaks in the fast and thermal neutron fluxes and power density are reduced, and located at a lower location in the core.

For a quick comparison with a  $UO_2$ -loaded core, although with a much lower discharge burn-up (96 MWd/kgHM), the thermal neutron flux and power density have been radially averaged (Figs. 5 and 6). It is shown that the flux with the  $PuO_{1.7}$  fuel is

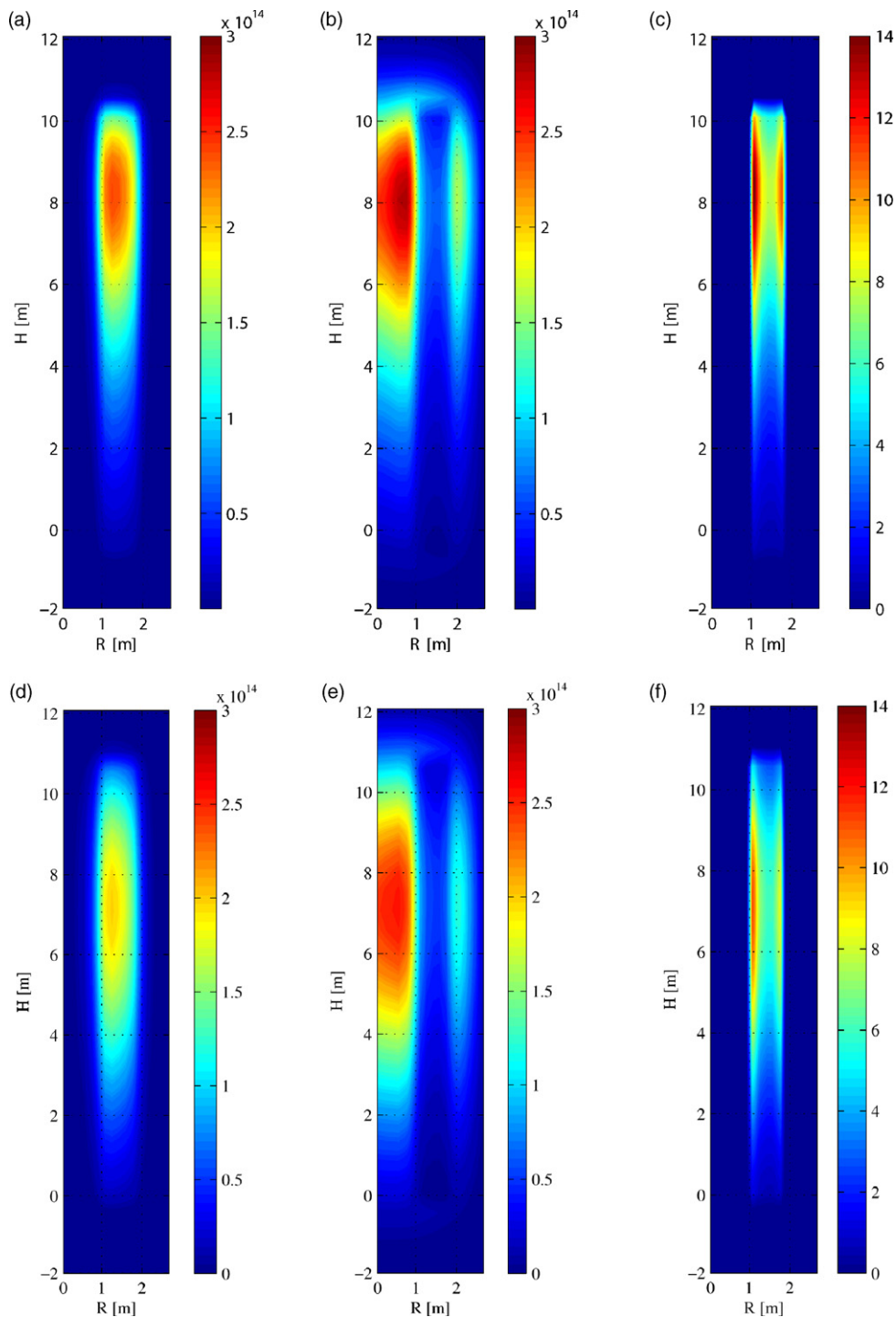


Fig. 4. (a and d) Fast and (b and e) thermal neutron fluxes ( $\text{cm}^{-2} \text{s}^{-1}$ ) and (c),(f) power density ( $\text{MW m}^{-3}$ ) in the core for the 1st and advanced reference fuels, respectively.

comparable to those with  $\text{UO}_2$ , in terms of shape and order of magnitude. As it could be expected, the thermal flux for the  $\text{PuO}_{1.7}$ -loaded core is lower than for the  $\text{UO}_2$ -loaded core due to the resonance absorption of Pu in the thermal energy range. In the case of the advanced reference fuel, the difference is more noticeable, as already mentioned from Fig. 4(b) and (e). However, the shape of the calculated thermal neutron flux would be expected in the case of a hypothetically infinite recycling scheme of the pebbles into the core. This is presently not the case, as the pebbles pass six times into the core before reaching their desired discharge burn-

up. This suggests to further investigate the calculation scheme, in which some approximations were made. In particular, the cross section generation script is performed in a way to provide accurate results with a reasonable computation time. This method proved to be effective with  $\text{UO}_2$  TRISO fuel kernels (Boer et al., 2008), but the presence in the fuel kernel of minor actinides with relatively high absorption cross sections may result in unexpected behaviors.

The same remarks also apply for the radially averaged power density profile shown in Fig. 6.

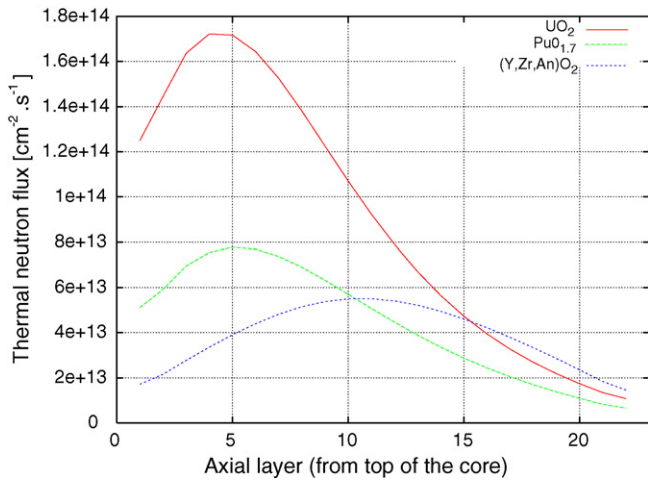


Fig. 5. Radially averaged thermal neutron flux in the core for UO<sub>2</sub>, PuO<sub>1.7</sub> and (Y,Zr,An)O<sub>2</sub> fuels.

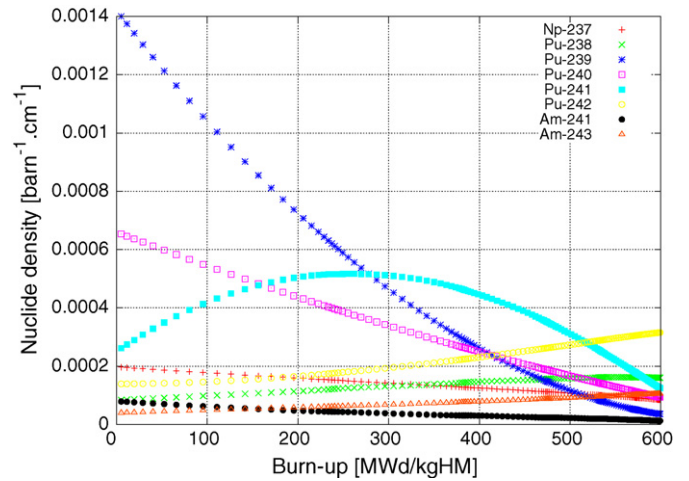


Fig. 8. Nuclide density evolution of the (Y,Zr,An)O<sub>2</sub> fuel during irradiation.

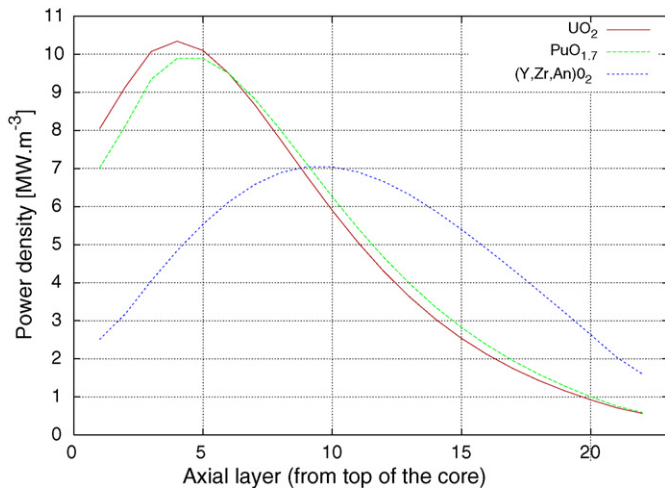


Fig. 6. Power density for UO<sub>2</sub>, PuO<sub>1.7</sub> and (Y,Zr,An)O<sub>2</sub> fuels.

### 4.3. Burning capabilities

The capability of the PBMR-400 reactor to burn plutonium and Minor Actinide isotopes during irradiation is now analysed. Fig. 7

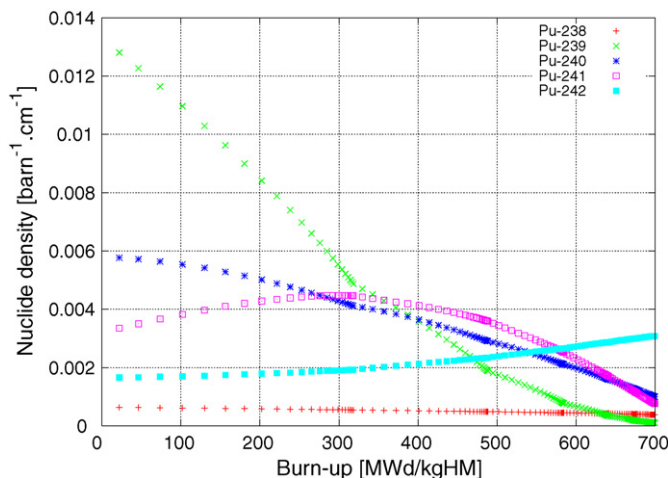


Fig. 7. Nuclide density evolution of the PuO<sub>1.7</sub> fuel during irradiation.

shows the evolution of plutonium isotopes during irradiation for the case of the 1st generation plutonium fuel. At 700 MWd/kgHM, the fuel is almost completely depleted from the plutonium fissile isotopes Pu<sup>239</sup> and Pu<sup>241</sup>.

Table 3 shows the isotopic vector for fresh and discharged 1st reference fuel. It is calculated that the fissile Pu-fraction is reduced from 66.98 down to 2.245 wt.% at 700 MWd/kgHM. Moreover, the discharged amount of Pu reduces to 22.98 wt.% of the original amount, while the total amount of actinides (U up to Cm) is reduced to 28.37 wt.%, as shown in Table 4.

The same results are presented for the advanced reference fuel. Fig. 8 also quantitatively shows a remarkable reduction of the initial minor actinide isotopes. Table 4 shows that the fissile Pu-fraction is reduced from 58.18 down to 5.611 wt.% (of initial heavy metal mass) at 600 MWd/kgHM. The discharged amount of Pu reduces to 25.39 wt.% of the original amount (88.98 wt.%), while the total amount of actinides (U up to Cm) is reduced to 35.55 wt.%.

The burning rates of plutonium and minor actinides that are initially present in the fuel and produced during irradiation are very promising for the use of the pebble-bed type HTR for transmutation purposes. It should be emphasised that this depends on the target discharge burn-up that can be achieved. Fig. 9 shows the burn-up of a pebble during irradiation. It is shown that the increase of the burn-up is rather small during the last two cycles (passes). However, the

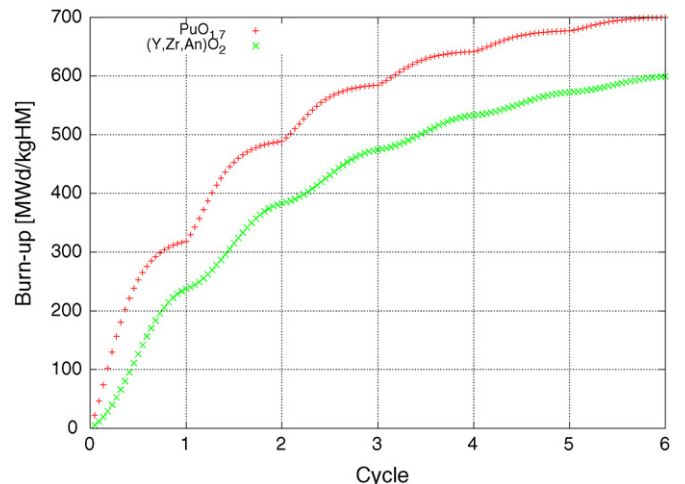


Fig. 9. Burn-up evolution during irradiation for both PuO<sub>1.7</sub> and (Y,Zr,An)O<sub>2</sub> fuels.

**Table 3**

Vectors of the fresh and discharged PuMA fuels (wt.% of initial heavy metal mass).

Fuel	Burn-up (MWd/kg)	Np-237	Pu-238	Pu-239	Pu-240	Pu-241	Pu-242	Am-241	Am-242m	Am-243
PuO <sub>1.7</sub>	0	0.0	2.59	53.85	23.66	13.13	6.78	0.0	0.0	0.0
	700	0.000787	1.228	0.206	5.494	2.039	14.010	0.138	~0.0	3.308
(Y,Zr,An)O <sub>2</sub>	0	6.8	2.9	49.38	23.0	8.8	4.9	2.8	0.02	1.4
	600	2.9489	5.5392	1.2472	3.2340	4.3748	10.995	0.4271	0.0129	3.6592

**Table 4**

Burning capabilities of the PuMA reference fuels (wt.% of initial heavy metal mass).

Fuel	Burn-up (MWd/kg)	U	Np	Pu	Am	Cm	Total
PuO <sub>1.7</sub>	0	0.0	0.0	100	0.0	0.0	100
	700	0.037	0.00079	22.98	3.447	1.901	28.37
(Y,Zr,An)O <sub>2</sub>	0	0.0	6.8	88.98	4.22	0.0	100
	600	0.0796	2.9502	25.3899	4.0992	3.0327	35.55

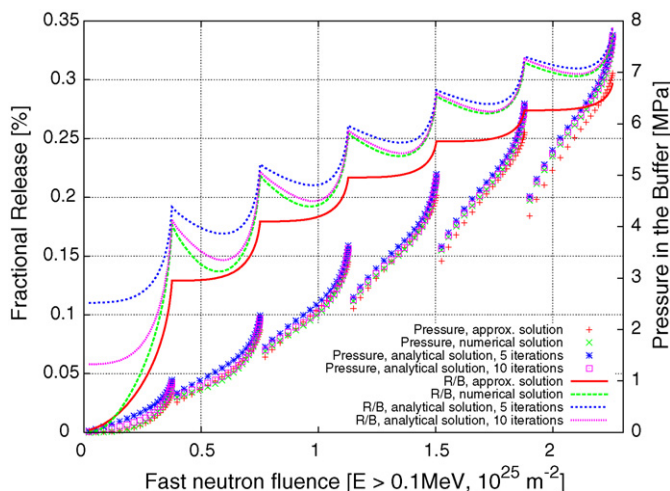
latter two cycles are very important for the reduction of plutonium and Minor Actinide densities, especially for the fissile <sup>241</sup>Pu isotope as shown in Figs. 7 and 8.

## 5. Fuel performance

The stress analysis code, as presented and detailed in Boer et al. (2008), was applied to the irradiation experiment of the first fuel loading of the HTTR (Sawa et al., 1996). The results for the tangential stress in the SiC layer obtained with the stress analysis code were in good agreement with the results obtained by Sawa et al. (1996) and the TIMCOAT code (Wang et al., 2004). The new developments presented in Section 3 are now implemented in a new version of the code, with which the following results were obtained when applied to Pu and PuMA-based TRISO particles.

### 5.1. Stress analysis

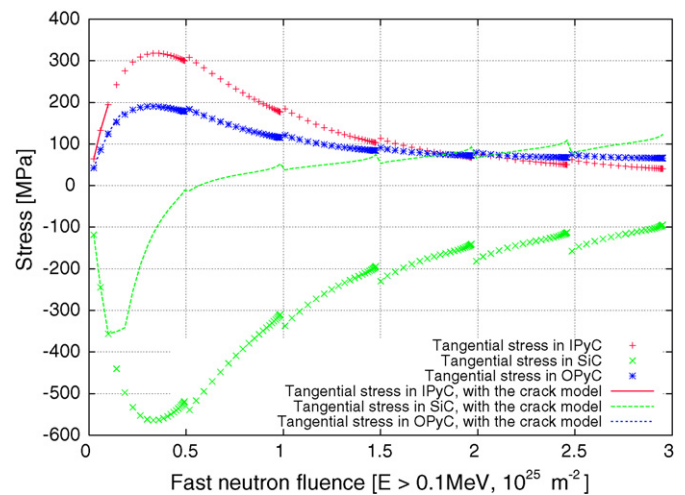
From the above equilibrium state results, various profiles such as fast neutron fluence, burn-up, pebble-surface temperature and inventory of stable fission gases are used as inputs for the stress analysis code. When running the CRYSTAL code, the fission gas release and the pressure in the buffer are calculated first. Fig. 10 shows typical fission gas release and pressure build-up profiles for the various models that are available in the CRYSTAL code. In the legend, “numerical solution” refers to the solution of Eq. (9) by use

**Fig. 10.** Typical Fission Gas Release and pressure profiles during irradiation.

of the finite difference method (Boer et al., 2008) and is considered here as the reference, “analytical solution” with 5 or 10 iterations refers to Eq. (20) with  $n = 5$  or 10, respectively, and “approx. solution” to Eq. (21).

Fig. 10 shows that the fission gas release as calculated with the analytical method with  $n = 10$  converges quickly to the numerical solution. With only five iterations, the error is relatively important at low fluence. However, this results in a very small discrepancy in the pressure profile, due to a low production of gaseous fission products at the beginning of irradiation. Inversely, the approximate solution for the fission gas release is in good agreement with the numerical solution at low fluence but rapidly deviates from it. This results in a lower buffer pressure as irradiation proceeds. In the next section, the sensitivity of both approximate and analytical solutions is investigated.

Once the buffer pressure is calculated, the calculation of the stress field in all coating layer is performed. Fig. 11 shows typical tangential stresses in the iPyC, SiC and oPyC layers. When the PyC layers are not allowed to crack, the SiC layer remains under compression for a very wide range of buffer pressure profiles. However, in case that any PyC layer fails, there is an important change in the stress of the SiC layer, which can become tensile. As a result, the SiC layer would be expected to fail once its tangential tensile stress becomes higher than its median strength. The effect of this change on the calculated failure fraction is also investigated.

**Fig. 11.** Typical mechanical behavior of a TRISO particle during irradiation, with and without the crack-induced failure model.

**Table 5**

Calculated failure fractions of  $\text{UO}_2$ ,  $\text{PuO}_{1.7}$  and  $(\text{Y,Zr,An})\text{O}_{1.7}$  fuel particles for different configurations of fission gas release and stress models.

Case	FGR	PyC failure	$\text{UO}_2$	$\text{PuO}_{1.7}$	$(\text{Y,Zr,An})\text{O}_{1.7}$
1	Analy. 5	Yes	$6.52 \times 10^{-5}$	$4.61 \times 10^{-2}$	$5.50 \times 10^{-6}$
2	Analy. 5	No	$< 10^{-7}$	$3.056 \times 10^{-4}$	$< 10^{-7}$
3	Approx	Yes	$3.54 \times 10^{-5}$	$2.31 \times 10^{-2}$	$2.80 \times 10^{-6}$
4	Approx	No	$< 10^{-7}$	$1.33 \times 10^{-5}$	$< 10^{-7}$
5	100%	Yes	$7.519 \times 10^{-4}$	$2.16 \times 10^{-1}$	$2.83 \times 10^{-5}$
6	100%	No	$< 10^{-7}$	$9.095 \times 10^{-4}$	$< 10^{-7}$

**5.2. Failure fractions**

By use of the stress analysis code, the calculation of failure fraction of TRISO particles during irradiation is investigated. For this purpose, it has been chosen to study the role of the fission gas release model and crack-induced failure model on the failure fraction. All sensitivity calculations have been performed for both reference fuels, and for  $\text{UO}_2$  as a reference.

Following the choice made in the past (Alberstein, 1994) for the 1st reference fuel, it has been proposed that the advanced reference fuel should be hypo-stoichiometric as well. The oxygen over metal ratio is arbitrary chosen to be  $\text{O/M} = 1.7$  for further reference. Practically, the hypo-stoichiometry is achieved during the fuel preparation by heating in hydrogen. The advantage in assuming an hypo-stoichiometric fuel composition is that the CO contribution in the buffer pressure build-up can be neglected. Moreover, it should be emphasised that Eq. (10) is only valid for U-based TRISO fuel (Nabielek et al., 2004; Proksch et al., 1982). As a result, the advanced reference fuel is now referred as  $(\text{Y,Zr,An})\text{O}_{1.7}$  in the following. The change in the oxygen content within the fuel kernel is not expected to change the results presented so far.

The results are shown in Table 5. In Table 5, “yes” and “no” means whether the crack-induced failure model is employed or not, and FGR refers to the fission gas release model used in the given case: 100% means that all stable gaseous fission products are instantaneously released into the buffer, “analy. 5” means that Eq. (20) is used with  $n = 5$ , and “approx” when Eq. (21) is used. The results shown in Table 5 enable to draw some conclusions:

- The impact of PyC-cracking on the behavior of the SiC layer, hence on the failure fraction can be analysed from cases 1, 3 and 5 with respect to cases 2, 4 and 6. When the crack-induced failure model is employed, this results in a failure fraction at least two orders of magnitudes higher than without the crack model. This shows clearly that attention must be put on the PyC layers when optimising the design of TRISO particles. However, it should be mentioned that no crack propagation through the SiC occurred in any of the TRISO particles which were predicted to fail. The failure of the SiC layer only occurred due to the change in the stress field as shown in Fig. 11, which eventually becomes tensile. Further validation of the crack model as proposed by Wang and Ballinger (2004) is therefore necessary. Indeed, it is not expected so many TRISO particles to fail in normal operating conditions. This conclusion is valid for the three fuel compositions.
- The pressure build-up in the buffer is one of the main sources of stress induced in the coating layers. Therefore, both calculations of production of gaseous fission products in the kernel and their release into the buffer are very important. Without the crack-induced failure model, the calculated failure fraction is too low to notice any difference between the FGR models. With the crack model, a comparison between cases 1, 3 and 5 shows that the failure fraction is sensitive to fission gas release. As shown in Fig. 10, the approximate solution given by Eq. (21) provides an underestimated buffer pressure, hence a lower failure fraction, with respect to the analytical solution provided by Kidson

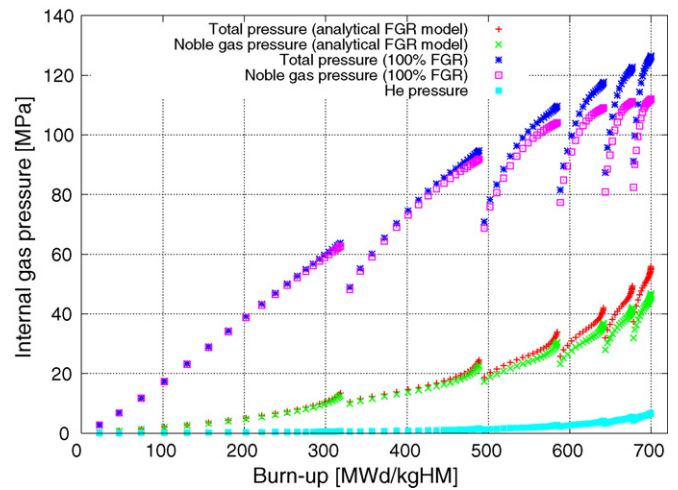


**Fig. 12.** Contribution of noble gas and helium in the total buffer pressure as a function of burn-up, calculated with the analytical FGR model or assuming instantaneous release (100%), for the 1st reference fuel.

Kidson (1980). Moreover, assuming 100% gas release (Wang et al., 2004) always leads to a higher and unrealistic failure fraction (compared to 35% for some sampled particles). Although the approximate solution or assuming 100% FGR can give quick results and an idea on the range of possible failure fractions, these models should not be used in fuel performance codes. This conclusion is valid for the three fuel compositions.

- As already emphasised in Section 3.4, the size of the sample is very important to obtain accurate results. Moreover, the sampling method is also very important, as shown from the results of cases 2, 4 and 6, where no TRISO particle is predicted to fail when  $10^7$  particles are sampled. In the current core physics code system used to calculate the equilibrium composition of a pebble-bed core, and on which the stress analysis code CRYSTAL is coupled, only one burn-up and five fast neutron fluence, power density and pebble surface temperature histories are available. As a consequence, it is expected that the calculated failure fractions may not be realistic enough. This suggests some improvements of the core physics codes in order to provide the stress analysis code with more realistic irradiation histories. This conclusion is valid for the three fuel compositions.

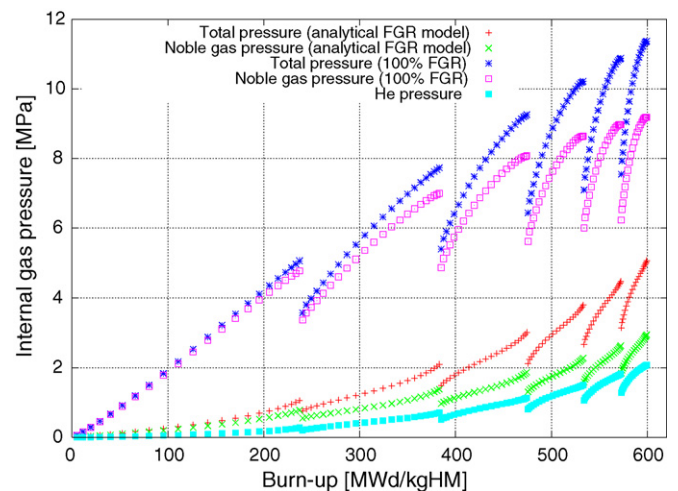


**Fig. 13.** Contribution of noble gas and helium in the total buffer pressure as a function of burn-up, calculated with the analytical FGR model or assuming instantaneous release (100%), for the advanced reference fuel.

- Due to the very high discharge burn-up and a smaller buffer layer, it is shown that the Pu-based fuel particles have a much higher failure fraction than the U and PuMA-based fuel particles. This is mainly due to the very high pressure that is induced in the buffer layer, as shown in Fig. 12. Although the calculated failure fractions are not verified against experimental results, the trend suggests that a new Pu-based fuel particle design should be proposed.
- On the contrary, the (Y,Zr,An)O<sub>1.7</sub> TRISO particles show much better performance. The dilution of the initial minor actinide content in a 500 μm diameter fuel kernel was chosen in such a way that the resulting bigger buffer layer would accommodate the amount of gaseous fission products and helium released (assumed to be 100% for helium) that contribute directly to the pressure build-up. Fig. 13 shows that this is achieved. The calculated failure fractions of the advanced reference fuel are similar to the ones of the standard UO<sub>2</sub> fuel.

## 6. Conclusions

A code system coupling core physics to stress analysis has been developed and applied to Pu and PuMA-based coated particle fuels in a PBMR-400 core design. The equilibrium fuel composition and fluxes have been calculated and are in good agreement with previous results. Fuel performance has been investigated by the calculation of TRISO particle failure fraction during irradiation, with particular attention to the effects of fission gas release and pyrocarbon failure on the mechanical behavior. It is shown that the first generation plutonium fuel particle design may not be the best option, due to a very high failure fraction even if the pyrocarbon layers are assumed not to fail during irradiation. On the contrary, the advanced reference fuel (recycled PWR spent fuel after five years of cooling, diluted in a yttria-stabilised zirconia inert matrix) particle shows a better performance. Although the calculated failure fractions are not verified against experimental results, the trend shows that the (Y,Zr,An)O<sub>1.7</sub> TRISO fuel can be considered as a good option, both from the transmutation capability and performance during irradiation points of view.

So far, most attention has been put on proposing a fuel kernel design in order to control the pressure build-up in the buffer layer. Concerning the geometry of the buffer and dense coating layers, the usual 90/40/35/40 μm thicknesses are still widely used. Historically, this combination seems to be a good choice although coming from not recent experimental research or from fuel performance codes that were not as developed as today's codes. Therefore, variations in this combination should be investigated, for instance by separately or both increasing the buffer layer thickness, decreasing the iPyC layer thickness and increasing the SiC layer thickness, in order to reduce the stress in all layers, hence the particle failure fraction. On the other hand, the fuel design optimisation should also consider the fabrication limitations and possible economic impacts.

Moreover, realistic models are only of worth when reliable materials data under irradiation conditions are available. In this sense, current international efforts are under way to gather all available data on material properties, share the data between research projects and to determine new data, especially at high temperature and under irradiation. This is the case for instance of the PYCASSO irradiation experiments (de Groot et al., 2008). This could make an important contribution to the fuel performance code development.

The stress analysis code CRYSTAL is still under development. Future improvements would include verification and validation of the crack-induced failure model proposed by Wang and Ballinger (2004) as a structural failure mechanism, but also take the Amoeba and chemical effects into account for the calculation of failure fractions. CRYSTAL could also be improved by use of an optimised

Monte Carlo sampling method, although mainly dependent to the irradiation histories provided by the core physics codes. Fuel performance should also be investigated during non-normal operating conditions, such as transient and accident conditions. For most of the advanced fuel performance codes, this is a very challenging point, but necessary for a complete description of fuel behavior during irradiation.

## Acknowledgements

The authors would like to acknowledge the support of the European Commission. The PUMA Project was carried out under contract no.036457 within the EURATOM 6th Framework Programme, effective from September 1, 2006 to August 31, 2009. The work reported in the present paper was done mainly during the post-doctoral research of the first author at Delft University of Technology, and finalised at Nuclear Research and Consultancy Group (NRG).

## References

- Alberstein, D., 1994. MHTGR Plutonium Consumption Study Phase II Final Report. Technical Report GA/DOE-051-94, General Atomics, April.
- Bacon, G.E., 1956. A method for determining the degree of orientation of graphite. *Journal of Applied Chemistry* 6, 477–481.
- Boer, B., Ougouag, A.M., Miller, G.K., Kloosterman, J.L., 2007. Mechanical stresses in fuel particles and graphite of high temperature reactors. In: Joint Int. Top. Meeting on Mathematics & Computation and Supercomputing in Nuclear Applications, 2007. Monterey, California, April 15–19.
- Boer, B., Ougouag, A.M., Kloosterman, J.L., Miller, G.K., 2008. Stress analysis of coated particle fuel in graphite of high temperature reactors. *Nuclear Technology*, 162.
- Boer, B., Lathouwers, D., Kloosterman, J.L., van der Hagen, T.H.J.J., Strydom, G., 2010. Validation of the DALTON-THERMIX code system with transient analyses of the HTR-10 and application to the PBMR. *Nuclear Technology* 170 (2), 306–321.
- CEGA Project, 1993. Np-mhtgr: Material Models of Pyrocarbon and Pyrolytic Silicon Carbide. Technical Report CEGA-002820, CEGA-Corporation.
- de Groot, S., 2008. RAPHAEL-FT & generation IV PYCASSO-I irradiation. In: Proceedings of the 4th International Topical Meeting on High Temperature Reactor Technology, Washington, DC, USA, September 28–October 1, 2008.
- de Haas, J.B.M., Kuijper, J.C., Oppe, J., 2006. Burn-up and transient analysis of a HTR-400 design loaded with PuO<sub>2</sub>. In: 3rd Int. Top. Meet. on High Temperature Reactor Technology, Johannesburg, South Africa, October 1–4, 2006.
- Grambow, B., Fachinger, J., Von, W., Lensa, 2007. Long term disposal of HTR fuel: leaching mechanism and experiments corrosion of graphite, coating layer and fuel. In: 2nd EC-RAPHAEL-PUMA Eurocourse on Coated Particle Fuel, Petten, The Netherlands, December 4–7, 2007.
- Heit, W., Huschka, H., Rind, W., Kaiser, G.G., 1984. Status of qualification of high-temperature reactor fuel element spheres. *Nuclear Technology* 69, 44–54.
- Hesketh, K., 2007. Non-proliferation aspects of high temperature reactors. In: 2nd EC-RAPHAEL-PUMA Eurocourse on Coated Particle Fuel, Petten, The Netherlands, December 4–7, 2007.
- I-NERI, 2004. Development for Improved Models and Designs for Coated Particle Gas Reactor Fuels. Technical Report INEEL/EXT-05-02615, INEEL.
- Jonnet, J., Kloosterman, J.L., Boer, B., 2008. Development of a stress analysis code for TRISO particles in HTRs. In: Int. Conf. on the Physics of Reactors, "Nuclear Power: A Sustainable Resource", Interlaken, Switzerland, September 14–19, 2008.
- Kidson, G.V., 1980. A generalized analysis of the cumulative delusional release of fission product gases from an "equivalent sphere" of UO<sub>2</sub>. *Journal of Nuclear Materials* 88, 299–308.
- Kuijper, J.C., 2007. PUMA—plutonium and minor actinides management in thermal high-temperature reactors. In: Int. Congress on Advances in Nuclear Power Plants, Nice, France, May 13–18, 2007.
- Kuijper, J.C., Raepsaet, X., de Haas, J.B.M., von Lensa, W., Ohlig, U., Ruetten, H.-J., Brockmann, H., Damian, F., Dolci, F., Bernnat, W., Oppe, J., Kloosterman, J.L., Cerullo, N., Lomonaco, G., Negrini, A., Magill, J., Seiler, R., 2004. HTR-N reactor physics and fuel cycle studies. In: 2nd Int. Top. Meet. on High Temperature Reactor Technology, Beijing, China, September 22–24, 2004.
- Michel, F., 2007. Mechanical modelling of HTR particles. In: 2nd EC-RAPHAEL-PUMA Eurocourse on "Coated Particle Fuel", Petten, The Netherlands, December 4–7, 2007.
- Mignanelli, M.A., 2008. Chemical Composition Optimisation for Pu and MA Kernels. PUMA Deliverable D216, February.
- Miller, G.K., 1995. Stresses in a spherical pressure vessel undergoing creep and dimensional changes. *International Journal of Solids and Structures* 32 (14), 2077–2093.
- Miller, G.K., 2006. Updated Solutions for Stresses and Displacements in Trisocoated Fuel Particles. Engineering Design File EDF-7042. Idaho National Laboratory.
- Miller, G.K., Bennett, R.G., 1993. Analytical solutions for stresses in trisocoated particles. *Journal of Nuclear Materials* 206, 35–49.

- Miller, G.K., Petti, D.A., Maki, J.T., Knudson, D.L., 2008. Updated solution for stresses and displacements in TRISO-coated fuel particles. *Journal of Nuclear Materials* 374, 129–137.
- Nabielek, H., Verföndern, K., Werner, H., 2004. Can we predict coated particle failure? A conversation on CONVOL, PANAMA and other codes. In: Technical Meeting on "Current Status and Future Prospects of Gas Cooled Reactor Fuels", IAEA, Vienna, June 7–9, 2004.
- Oku, T., Ishihara, M., 2004. Lifetime evaluation of graphite components for HTGRs. *Nuclear Engineering and Design* 227, 209–217.
- Oku, T., Eto, M., Ishiyama, S., 1990. Irradiation properties and strength of a fine-grained isotropic graphite. *Journal of Nuclear Materials* 172, 77–84.
- Olander, D.R., 1976. *Fundamental Aspects of Nuclear Reactor Fuel Elements*. Technical Information Center, Energy Research and Development Administration.
- ORNL SCALE: a modular code system for performing standardized computer analysis for licensing evaluations. ORNL/TM-2005/39, version 5, vols I–III. Oak Ridge National Laboratory, Tennessee, USA, April 2005.
- Proksch, E., Strigl, A., Nabielek, H., 1982. Production of carbon monoxide during burn-up of UO<sub>2</sub> kerneled HTR fuel particles. *Journal of Nuclear Materials* 107 (28).
- Sawa, K., Shiozawa, S., Minato, K., Fukuda, K., 1996. Development of a coated fuel particle failure model under high burnup irradiation. *Journal of Nuclear Science and Technology* 33 (9), 712–720.
- Smith, J.M., van Ness, H.V., Abbott, M.M., 2001. *Introduction to Chemical Engineering Thermodynamics*. McGraw-Hill. ISBN 0-07-118957-2.
- Somers, J., 2007. Plutonium and Minor Actinide Fuels for HTR. PUMA Deliverable D211, January.
- Somers, J., Fernandez, A., 2006. Inert matrix kernels for actinide incineration in high temperature reactors. *Progress in Nuclear Energy* 48, 259–267.
- Somers, J., Fernandez, A., 2007. Novel Inert Matrix Fuel Kernels for Pu and Minor Actinide Incineration in High Temperature Reactors. In: Petten, The Netherlands, December 4–7, 2007.
- Struth, S., 1995. Thermix-Direkt: Ein Rechenprogramm zur instationären zweidimensionalen Simulation thermohydraulischer Transienten. Fz jülich, Germany.
- Timoshenko, S.P., Goodier, J.N., 1970. *Theory of Elasticity*, 3rd edition. McGraw-Hill Inc.
- Walter, M., N/"astren, C., Somers, J., Jardin, R., Denecke, M.A., Brendebach, B., 2007. Local atomic structure of a zirconia-based americium transmutation fuel. *Journal of Solid State Chemistry* 180, 3130–3135.
- Wang, J., 2004. An integrated performance model for high temperature gas cooled reactor coated particle fuel. PhD thesis, Massachusetts Institute of Technology.
- Wang, J., Ballinger, R.G., 2004. Fracture mechanics based coated particle fuel failure models. In: 2nd Int. Top. Meet. on High Temperature Reactor Technology, Beijing, China, September 22–24, 2004.
- Wang, J., Ballinger, R.G., Maclean, H.J., 2004. TIMCOAT: an integrated fuel performance model for coated particle fuel. *Nuclear Technology* 163, 68–96.